Lattice thermal conductivity of MgO at conditions of Earth's interior

Xiaoli Tang[a,b,1] and Jianjun Dong[a]

[a]Physics Department, Auburn University, 206 Allison Lab, Auburn University, Auburn, AL 36849 and [b]Earth and Space Science Department, University of California, Los Angeles, 595 Charles Young Drive East, Box 951567, Los Angeles, CA 90095

Edited by Russell J. Hemley, Carnegie Institution of Washington, Washington, DC, and approved January 11, 2010 (received for review June 26, 2009)

Thermal conductivity of the Earth's lower mantle greatly impacts the mantle convection style and affects the heat conduction from the core to the mantle. Direct laboratory measurement of thermal conductivity of mantle minerals remains a technical challenge at the pressure-temperature (P-T) conditions relevant to the lower mantle, and previously estimated values are extrapolated from low P-T data based on simple empirical thermal transport models. By using a numerical technique that combines first-principles electronic structure theory and Peierls–Boltzmann transport theory, we predict the lattice thermal conductivity of MgO, previously used to estimate the thermal conductivity in the Earth, at conditions from ambient to the core-mantle boundary (CMB). We show that our first-principles technique provides a realistic model for the P-T dependence of lattice thermal conductivity of MgO at conditions from ambient to the CMB, and we propose thermal conductivity profiles of MgO in the lower mantle based on geotherm models. The calculated conductivity increases from 15–20 W/K-m at the 670 km seismic discontinuity to 40–50 W/K-m at the CMB. This large depth variation in calculated thermal conductivity should be included in models of mantle convection, which has been traditionally studied based on the assumption of constant conductivity.

first-principles | phonon transport theory | phonon lifetime | high pressure | Lower Mantle

Thermal conductivity (κ) is one of the most important mineral properties in determining the heat budget of the Earth. Heat in the Earth's interior is transferred by convection in the mantle and core and regulated by conduction at thermal boundary layers. As defined by Fourier's law of heat conduction $J_Q = -\kappa \cdot \nabla T$, determines the conducting heat flow density (J_Q) in the presence of a temperature gradient ∇T. κ also appears in the Rayleigh number, which measures the convective vigor of a system. Thus, the thermal conductivity of the lower mantle affects the structure, thickness, and dynamics of the CMB (1, 2), the style and structure of mantle convection (3–5), and the amount of heat conducted from the core to the mantle (6) that in turn influences the generation of the Earth's magnetic field (7).

Despite its importance, thermal conductivity remains as one of the least constrained physical properties of minerals, especially at lower-mantle pressures (P) and temperatures (T) (23–135 GPa (8) and approximately 1,900–4,000 K (9–12). Experimental data at deep mantle conditions are scarce due to the technical difficulty of measuring thermal conductivity at these extremes. Thermal conductivity of lower-mantle minerals is often estimated either by extrapolating data from lower P-T conditions and/or employing theoretical models with parameters fitted with lower P-T data (1, 13). However, direct extrapolation to deep mantle conditions can be unreliable beyond the P-T range of the measurements, and empirical models are often based on untested assumptions. For example, the sound velocities are used to approximate phonon velocities, and the pressure dependence of phonon lifetime is assumed to be given by equilibrium thermodynamic properties, such as lattice thermal expansion and/or Grüneisen parameters.

MgO, the end-member of the second-most abundant mineral in the lower mantle, has historically served as a model system for evaluating the thermal conductivity of the deep mantle (14). Its thermal conductivity is also an order of magnitude larger than that of Mg end-member of the most abundant mantle mineral—silicate perovskite (15). Hence, studying its thermal conductivity provides a useful approach to constraining the thermal conductivity of the lower mantle. Though efforts have been devoted to measuring the thermal conductivity of MgO (κ_{MgO}) at both high pressures and temperatures (16–24), most of those measurements have been limited to below 7 GPa. First, nonempirical calculations of lattice thermal conductivity (25) of MgO at high pressure were performed based on molecular dynamics simulations and Green–Kubo theory (26). An order of magnitude underestimation of κ_{MgO} in that study is maybe due to the ionic potential model adopted in the simulation that does not adequately account for lattice anharmonicity.

In this paper, we report a first-principles study of the lattice thermal conductivity of MgO in the pressure and temperature ranges of 0–150 GPa and 300–4,000 K, respectively. Our method combines first-principles lattice vibration calculations, quantum phonon scattering theory, and Peierls–Boltzmann transport equation within the single-mode excitation approximation. We first investigate the microscopic heat transport characteristics of all the acoustic and optic phonons and examine the density and temperature dependence of κ_{MgO}. We then determine κ_{MgO} at lower-mantle pressures and temperatures with the thermal equation of state predicted from our first-principles calculations. Finally, we propose a depth profile of κ_{MgO} in the lower mantle based on previous estimates of cold and hot geotherms.

Results

To predict the lattice thermal conductivity of MgO crystals at conditions from ambient to those of the Earth's CMB, we first computed the harmonic force constant matrices of lattice vibration and the third-order lattice anharmonicity tensors at seven densities, ranging from 3.35 to 5.15 g/cm^3 (27). At each density, we explicitly evaluated phonon scattering rates of all the irreducible phonon modes at nine temperature points from 300–4,000 K. Finally, we derived microscopic phonon mode conductivity $\kappa(i,\vec{q}) = \frac{1}{3}c_V(i,\vec{q})v_g^2(i,\vec{q})\tau(i,\vec{q})$ using the calculated heat capacity c_V, group velocity v_g, and scattering rate/lifetime τ of each phonon mode $(i,\vec{q})$ on a $16\times16\times16$ $\vec{q}$-point Brillouin zone grids for all the 63 density-temperature configurations.

Fig. 1 shows our calculated average mode conductivity κ_{mode} for phonons within different phonon frequency (ω) ranges at $\rho =$ 3.70 g/cm^3 and $T = 300$ K. While all phonons transfer heat, the lower frequency acoustic modes are clearly much more efficient

Author contributions: X.T. and J.D. designed research, performed research tools, analyzed data, and wrote the paper.

The authors declare no conflict of interest.

This article is a PNAS Direct Submission.

[1]To whom correspondence should be addressed. E-mail: xtang@igpp.ucla.edu.

This article contains supporting information online at www.pnas.org/cgi/content/full/0907194107/DCSupplemental.

GEOPHYSICS

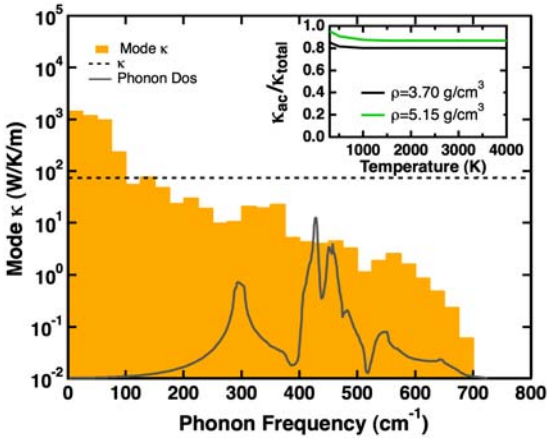

Fig. 1. The semilog histogram plot of the averaged mode κ (with $\Delta\omega = 20$ cm^{-1}) for phonon modes at different frequency ranges for MgO at the density of 3.70 g/cm^3 and temperature of 300 K. The averaged mode κ of phonons decreases rapidly with increase of phonon frequency. κ_{mode} of acoustic phonon modes near the Brillouin zone center (i.e., at the lowest 60 cm^{-1} frequency region) is about two orders of magnitude larger than those of acoustic phonon modes around the zone boundaries (between 300 cm^{-1} to 400 cm^{-1}), and more than four orders of magnitude larger that those of longitudinal optic modes around the zone center (above 650 cm^{-1}). The *Horizontal Dashed Line* indicates the value of bulk κ. Although there are equal numbers of acoustic and optic phonon modes, the overall contribution of optic phonons at the high temperature limit only accounts for about 15% and 14% in total lattice thermal conductivity at the density of 3.70 g/cm^3 and 5.15 g/cm^3 resp. (*Inset*).

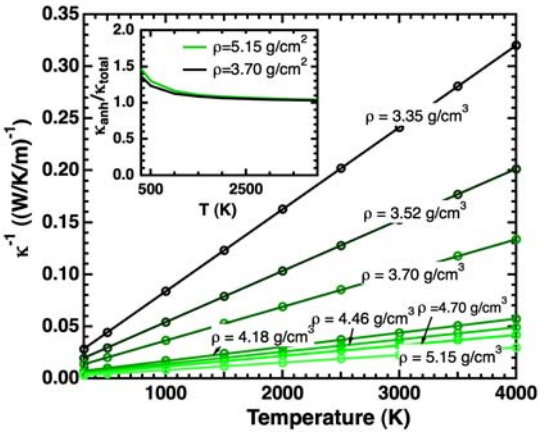

Fig. 2. The inverse of lattice thermal conductivity of MgO crystal scales consistently as a linear function of temperature, from 300– 4,000 K, at the constant density condition. The calculated κ results from two phonon scattering mechanisms—the temperature-dependent, anharmonicity-induced phonon scattering and the temperature-independent, isotope-induced scattering. The isotope effect on the total κ is illustrated in the inset for results from 300–4,000 K at two densities.

in heat conduction than the higher frequency optic modes. This is consistent with the fact that the acoustic modes, especially those near the Brillouin zone center, have much larger group velocities than optical modes. For modes near zone center, we find that the ratio between acoustic and optic group velocities can be as large as 12. Furthermore, our calculations reveal that the average phonon lifetime of acoustic phonons is approximately a factor of threelonger than those of optic phonons. MgO crystalline with only two atoms per unit cell, contain equal numbers of acoustic branches and optic branches. Yet, the overall contribution of acoustic phonons accounts for nearly 85% of the total thermal conductivity at 300 K (Fig. 1 *Inset*). This ratio deceases slightly with increasing temperature as more optic phonons are thermally excited, and it approaches 80% above the Debye temperature. The high temperature limit of $\kappa_{acoustic}/\kappa_{total}$ increases mildly under large compression (for example, about 87% at $\rho = 5.15$ g/cm^3).

Fig. 2 presents our theoretical prediction of the temperature dependence of lattice thermal conductivity of MgO at selected densities. The inverse of the calculated lattice thermal conductivity κ_{MgO}^{-1} scales consistently as a linear function $(A + BT)$ over the entire calculated temperature range (from 300–4000 K) when *density* is held constant. This predicted linear temperature dependence of $1/\kappa$ can't be extended to low temperature as our calculations do not take into account the scattering mechanisms (such as point defects, dislocations, or grain boundary scattering) that are much less important at temperature conditions relevant to the Earth's hot interior. For instance, Gibert et a.l (28) has studied experimentally the effect of grain boundary scattering on the thermal diffusivity. By comparing the measured thermal diffusivity of both single crystal and polycrystalline olivine (with grain sizes varying from 0.01– 2 mm), they concluded that the grain boundary scattering has a negligible effect on thermal diffusivity at ambient conditions. To extend this finding to elevated temperatures and pressures (larger density), we adopt a simple empirical model of Callaway (29) and find that grain boundaries of polycrystalline MgO start to play a role at ambient condition only if the characteristic length l is in the order of μm or smaller. Taking $l = 1$ μm for example, the estimated reduction in κ_{MgO} due to grain boundary scattering is 13% and 26% at room temperature for density of 3.70 g/cm^3 and 5.15 g/cm^3, resp., and they are significantly lower at 2,000 K and become only 2% and 2.6%, resp. A similar trend is also found in our modeling of defect scattering. Hence, we conclude that it is valid to neglect the effect of defects and boundary scattering in studying the thermal conductivity of Earth's hot interior, and phonon–phonon interaction is the major scattering process that hinders the heat transport at high temperatures.

In this study, the temperature-independent A term mainly represents the contribution associated with the mass disorder (i.e., isotope) induced phonon scattering (30). As shown in the *Inset* of Fig. 2, the neglection of isotope-induced phonon scattering leads to a noticeable overestimation of thermal conductivity around ambient temperature. At 300 K, this can lead to an overestimation as large as 46% for $\rho = 3.70$ g/cm^3. However, the contribution of the isotope effect diminishes at high temperature—falling to 4% at 4000 K at the same density. This reveals that it is necessary to include the isotope effect when one compares the $\kappa(T)/\kappa(T = 300\text{ K})$ ratio between measurements and calculations. The temperature-dependent BT term can be primarily attributed to the anharmonicity-induced 3-phonon scattering mechanism that dominates at high temperature, and lattice thermal conductivity approaches to the well-known $\kappa \propto \frac{1}{T}$ relation at the high-T limit (31). As both A and B terms are non-negatively defined, we fitted the log functions of A and B terms of the seven studied densities with second order polynomial functions of $1/\rho$:

$$\kappa^{-1}(T,\rho) = A(\rho) + B(\rho)T = \exp\left[a_0 + \frac{a_1}{\rho} + \frac{a_2}{\rho^2}\right] + \exp\left[b_0 + \frac{b_1}{\rho} + \frac{b_2}{\rho^2}\right] \cdot T. \quad [1]$$

The fitting parameters are listed in Table 1.

Discussion

We first compare our results with available experiments, which are performed under either ambient pressure or room temperature conditions. Based on the proposed density-temperature model (Eq. **1** and Table 1), κ_{MgO} at isobaric conditions can be readily obtained with the thermal equation of state $\rho(T,P)$. Fig. 3 shows the calculated $\kappa_{MgO}(T,P)$ at ambient pressure based on our calculated (*Solid Line*) and measured (*Dashed Line*) equation of

Table 1. Fitting parameters of thermal conductivity of MgO as a function of density (ρ) and temperature (T) shown in Eq. 1. The adopted units for κ, T, and ρ are W/K-m, K, and g/cm^3, resp.

a_0	a_1	a_2	b_0	b_1	b_2
−17.50000	80.07815	−132.02510	−9.30500	−35.90633	118.58743

state (32), in comparison with four sets of experimental data (16–18, 23, 33) in symbols. Our predicted κ_{MgO} at 300 K is about 66 W/K-m, which is in agreement with the reported experimental data scattering from 36 to 70 W/K-m. A detailed review of experimental data for κ_{MgO}, including systematic errors in various techniques and qualities of measured samples, can be found in ref. 13. The adopted first-principles local density approximation (LDA) theory is known to overestimate density, and we find adopting the experimental equation of state (32) lowers our calculated κ_{MgO} by about 10%. Nevertheless, our calculations in general slightly overestimate κ, and this is consistent with the fact that all experimental samples are of small sizes and contain intrinsic imperfections, whereas calculations assume perfect crystallinality. While decreasing with temperature, lattice thermal conductivity increases under compression. The *Inset* of the Fig. 3 shows the calculated $\kappa(P)/\kappa(P=0)$ ratio at 300 K (*Solid Line*) that falls in the scattered experimental high pressure measurements (19–22). The LDA-calculated isothermal pressure coefficient ($d\ln(\kappa_{MgO})/dP$) is about 3.90% GPa^{-1} at $T = 300$ K near ambient pressure, which is in good agreement with the measured value of 4% GPa^{-1} (20, 33) and 4.9% GPa^{-1} (21).

Due to the lack of direct measurements at deep mantle conditions, various empirical models (1, 33, 34) have been proposed to describe the relative change in thermal conductivity upon compression to extrapolate experimental data to the relevant pressure conditions of the Earth's interior. Most of these models are based on the simple empirical expression of $\kappa = \frac{avB_T}{3\gamma^2 T}$ proposed by Dugdale and McDonald (35), where a is the interatomic distance, v is the averaged phonon velocity, B_T is the isothermal bulk modulus, and γ is the Grüneisen parameter. Additional approximations are often adopted to describe the density dependency of these relevant thermal properties. For example, Poirier (34) derived $d\ln(\kappa)/dP = (2\gamma + 5/3)/B_T$. Hofmeister (36) proposed a damped harmonic oscillator (DHO) model that originates directly from the microscopic phonon transport theory (Eq. **2**).

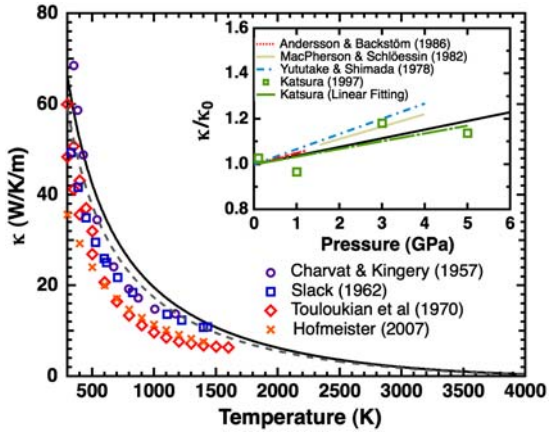

Fig. 3. Comparison between calculation and experiment for κ_{MgO} at ambient pressure. Our calculated $\kappa_{MgO}(T)$ at ambient pressure, based on the LDA calculated (*Solid Curve*) and experimentally measured (*Dashed Curve*) thermal equation of state (32), are in good agreement with previous experimental measurements from refs. 16–18 and 23 (*Symbols*). Underestimation of equilibrium density from LDA calculations leads to ~10%. The *Inset* shows the data of calculated and measured κ_{MgO} (19–22) as a function of pressure (up to 6 GPa) at room temperature.

However, because of the insufficient experimental data on individual phonon modes (such as their group velocities and lifetimes), further simplifications are inevitable for studying real minerals. The simplified DHO model predicts the upper limit of the $d\ln(\kappa)/dP$ coefficient as $(4\gamma + 1/3)/B_T$ (23).

To compare our first-principles results with empirical models, we first calculated $d\ln(\kappa_{MgO})/dP$ based on the above two empirical models by using our LDA-calculated γ and B_T (Fig. 4*A* and *B*), and then derived their $\kappa(P)/\kappa_o$ ratio by integration (Fig. 4*C* and *D*). The simplified DHO-model-predicted $d\ln(\kappa_{MgO})/dP$ at 300 K and ambient pressure is in agreement with our first-principles calculation. However, our calculated $d\ln(\kappa_{MgO})/dP$ decays faster under compression than that predicted by the simplified DHO model, and incidentally approaches the prediction of the Poirier model at higher pressures (Fig. 4*A*). Consequently, the $\kappa(P)/\kappa_o$ ratio predicted by the Poirier model is closer to that calculated with our first-principles method, whereas the predictions by the simplified DHO model are more than 20% larger at pressures higher than 80 GPa (Fig. 4*C*). The incidental agreement between the Poirier model and our first-principles calculations does not hold for all temperatures. For example, at 3,000 K our calculated $d\ln(\kappa_{MgO})/dP$ is significantly higher than that predicted by empirical models at ambient pressure (Fig. 4*B*), and the difference in the prediction of $\kappa(P)/\kappa_o$ between empirical models and current calculations becomes more significant at higher temperatures and pressures (Fig. 4*D*). Our results suggest that such empirical models are inadequate even for structurally simple minerals like MgO, and they are more likely to yield larger uncertainties for complex minerals such as silicate perovskite. Furthermore, we find that temperature has a strong effect on the pressure derivative $d\ln(\kappa_{MgO})/dP$. It increases rapidly with the increase of temperature at pressures lower than 50 GPa, and becomes almost temperature independent above 80 GPa. At CMB conditions ($P = 135$ GPa and $T = 3,000$ K), our first-principles calculations predict κ_{MgO} and $d\ln(\kappa_{MgO})/dP$ to be around 43 W/K-m and 0.36% GPa^{-1}, resp.

The geotherm of the Earth's lower mantle depends on the thermal conductivity of the lower mantle. In the current study, we adopt a hot and cold geotherm based on experimental constraints (37) to give a direct estimation of κ_{MgO} at the

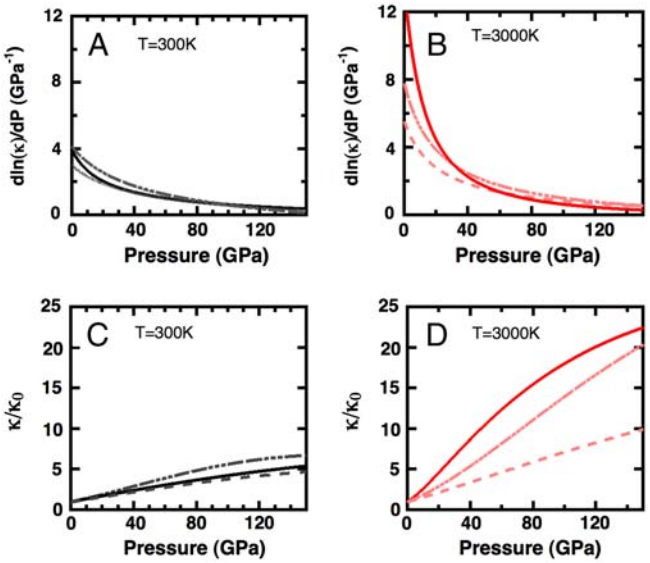

Fig. 4. Pressure derivatives $d\ln(\kappa_{MgO})/dP$ and isothermal $\kappa(P)/\kappa(P=0)$ ratios as functions of pressure: (*A*) $d\ln(\kappa_{MgO})/dP$ at 300 K, (*B*) $d\ln\kappa/dP$ at 300 K, (*C*) $\kappa(P)/\kappa(P=0)$ at 3,000 K, and (*D*) $\kappa(P)/\kappa(P=0)$ at 300 K. Our first-principles results are plotted in *Solid Curves*, compared with previous empirical models: *Dashed-Dotted Curve* for Hofmeister's simplified DHO model (23) and *Dashed Curve* for Poirier's model (34).

lower-mantle conditions (Fig. 5). The cold geotherm corresponds to whole-mantle convection, whereas the hot geotherm to partially-layered convection. Large differences between the hot and cold geotherms are due to the uncertainties in the temperature structure as well as the lateral inhomogeneity. Nevertheless, these two geotherms provide a reasonable temperature bound for the lower mantle. At the same depth, κ_{MgO} can be 5–10 W/K-m lower along the hot geotherm than along the cold geotherm. However, it holds true that κ_{MgO} changes greatly with depth, from 15–20 W/K-m at the 670 + km transition zone to 40–50 W/K-m on the mantle side of the CMB. The calculated depth dependence of κ_{MgO} along the hot and cold geotherms above the CMB are $\kappa^{hot}_{MgO}(z) = 15.753 + 0.01844 \cdot z - 3.142 \cdot 10^{-6} \cdot z^2$ and $\kappa^{cold}_{MgO}(z) = 21.421 + 0.01844 \cdot z - 3.768 \cdot 10^{-6} \cdot z^2$ resp., where z (in the unit of km) is the depth in the lower mantle relative to the 670 km seismic discontinuity. An 800 K-temperature difference across the CMB layer can reduce κ_{MgO} from 43 W/K-m to 34 W/K-m, indicating depth dependence of thermal conductivity within the layer should not be neglected when one considers the heat conduction at the boundary layer; e.g., it affects the thickness of the thermal boundary layer δD through $\int_0^{\delta D} \frac{q}{\kappa(z)} dz = \Delta T$ for a heat flux from the core of q.

Our current first-principles calculations represent an improvement in modeling the lattice thermal conductivity of this model oxide material. Several key issues need to be resolved to realistically constrain the thermal conductivity of the lower mantle, which is mainly controlled by the composite-averaged thermal conductivity of (Mg,Fe)O and $(Mg,Fe)SiO_3$. First, the effect of iron in mineral solid solutions is important yet poorly understood. The iron content not only modifies the density, interatomic forces, and lattice anharmonicity but also adds microscopic disorder. Our first-principles technique can be expanded to include this effect, but this is beyond the scope of this study. A preliminary analysis reveals that the key effect is a significant reduction of phonon group velocities with increasing iron contents. Effects associated with the Fe-Mg mass disorder, although significant at 300 K, diminish with increasing temperature. A quantitative evaluation of iron effects requires more comprehensive theoretical treatment.

Second, accurate modeling of composite-averaged thermal conductivity requires knowledge of the thermal conductivity of both the individual constituents and the structures of the composite. The perovskite end-member ($MgSiO_3$) is known to have a much lower thermal conductivity than the magnesiowüstite end-member (MgO). At ambient conditions, the thermal conductivity of $MgSiO_3$ perovskite is 5.1 W/K-m (38), which is less than 10% of that of MgO. If $MgSiO_3$ perovskite behaves similarly to MgO upon heating and compression, we estimate that the upper bound of the thermal conductivity at the top of the CMB will be around $11 \sim 12$ W/K-m, assuming that MgO and $MgSiO_3$ are layered side-by-side along the direction of heat flow (39). More realistic composite structures should be included in future studies, along with better constraints on the thermal conductivity of silicate perovskite and the effects of iron content in solid solution at lower-mantle conditions.

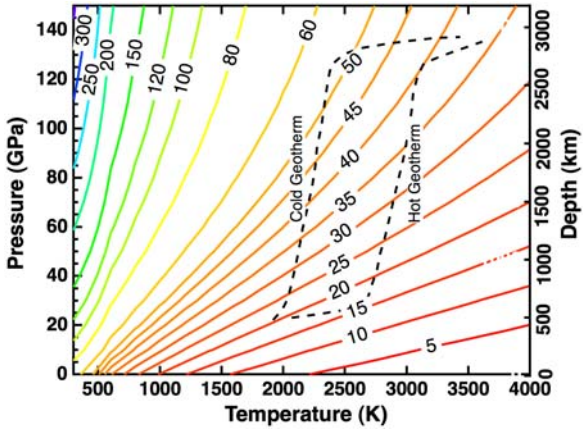

Fig. 5. Pressure and temperature contour plot of the lattice thermal conductivity of MgO. *Dashed Lines* are estimated cold and hot geotherms from experiments (37).

Finally, in the Earth's hot interior, an additional effective thermal conductivity due to the inter-grain thermal radiation can be considered. Radiative thermal conductivity increases rapidly with increasing temperature, and becomes significant at high temperatures (40, 41). On the other hand, the effect of radiative heat transfer is diminished with the reduction of grain size; it is also controlled by the iron concentration of the minerals (42). Optical absorption measurements at high pressure have been used to infer the radiative thermal conductivity of lower-mantle minerals (43–46). Large discrepancies were found among the estimates of radiative thermal conductivity from these measurements that might be due to the differences in sample grain size, iron concentration, or different experimental setups. Further experimental investigation is needed to constrain the average radiative thermal conductivity at conditions near the CMB, including the contribution due to the high-spin/low-spin transition.

Method

Many microscopic processes contribute to the overall heat conduction in a solid. For insulating mantle minerals, heat conducts mainly via lattice vibrations (31). The Peierls–Boltzmann transport equation expresses the lattice thermal conductivity as:

$$\kappa = \frac{V_o}{8\pi^3} \sum_{i=1}^{3N_a} \int_{BZ} \left[\frac{1}{3} c_V(\vec{q},i) v_g(\vec{q},i) d(\vec{q},i) \right] d\vec{q}$$
$$= \frac{V_o}{8\pi^3} \sum_{i=1}^{3N_a} \int_{BZ} \left[\frac{1}{3} c_V(\vec{q},i) v_g^2(\vec{q},i) \tau(\vec{q},i) \right] d\vec{q}, \qquad [2]$$

where V_o is the volume of the unit cell, N_a is the number of atoms in the unit cell, and the integration is over the first Brillouin zone in the reciprocal $\vec{q}$-space. Each phonon mode in the $\vec{q}$-space is labeled with its crystal momentum $\vec{q}$ and polarization index i (from 1 to $3N_a$), and c_V, v_g, τ, and $d = v_g\tau$ are its heat capacity, phonon group velocity, phonon lifetime, and phonon mean free path, resp.

The first-principles local density approximation techniques are now routinely adopted to accurately predict harmonic lattice phonon spectra that can be readily used to derive phonon heat capacity and group velocity in Eq. **2**. To evaluate phonon lifetime τ, we consider two types of perturbation to the nearly independent phonon model—the third-order lattice anharmonicity and the isotope mass disorder. The phonon scattering rate $(\Gamma(\vec{q},i))$ that is the inverse of $\tau(\vec{q},i)$, can be calculated from Fermi's Golden rule: $\Gamma_i^f = \langle \Phi_f | \delta H | \Phi_i \rangle$, where Γ_i^f is the transition rate from the initial state Φ_i to the final state Φ_f of a many-phonon system under perturbation δH. In the present study, instead of directly solving for the phonon distributions at the presence of temperature gradients, we further adopt the single-mode excitation approximation to evaluate the relaxation rate of a phonon mode when only this phonon mode is perturbed out of its thermal equilibrium (47). Each type of phonon scattering is treated individually, and the overall transition rate is approximated as the sum of all the transition rates from different scattering mechanisms [Matthiessen's rule (48)]. More details of the phonon lifetime calculations are provided in *SI Text*.

Conclusions

The first-principles-derived model has been developed to advance our understanding of lattice thermal conductivity of minerals at deep mantle conditions. By combining the microscopic transport theory and first-principles lattice dynamics calculations, we have predicted the value for MgO over a broad range of P-T conditions of the lower mantle without empirical extrapolation. The good agreement with low P-T measurements suggests that the first-principles-based implementation of Peierls–Boltzmann transport theory within single-mode excitation approximation can be used to predict the thermal conductivity of insulating mantle minerals at high P-T conditions. Our study indicates that the calculated values for MgO vary significantly with depth in the lower mantle, increasing by a factor of 2–3 from the 670 km discontinuity (15–20 W/K-m) to the mantle side of the CMB (40–50 W/K-m). This finding starkly contrasts with the assumption of constant thermal conductivity that is widely adopted in many geodynamics simulation studies of the lower mantle. Our first-principles technique could be readily adapted to study lattice thermal conductivity of iron-bearing lower-mantle minerals. In light of further improved experimental data of lattice thermal conductivity at lower pressure (49) and radiative thermal conductivity at the condition of the CMB, our study should serve as a useful stepping stone to realistically constrain the total thermal conductivity of the lower mantle.

ACKNOWLEDGMENTS. We thank A. Kavner, A.M. Hofmeister, D.A. Drabold, and G. Poirier for helpful discussions and R.J. Hemley and anonymous reviewers for comments and suggestions. This work is supported by National Science Foundation Grants EAR-0757847 and EAR-0510914.

1. Brown JM (1986) Interpretation of the D′′ zone at the base of the mantle—Dependence on assumed values of thermal-conductivity. *Geophys Res Lett* 13:1509–1512.
2. Naliboff JB, Kellogg LH (2007) Can large increases in viscosity and thermal conductivity preserve large-scale heterogeneity in the mantle?. *Phys Earth Planet In* 161:86–102.
3. Turcotte DL, Schubert G (1982) *Geodynamics—Applications of Continuum Physics to Geological Problems* (Cambridge Univ Press, Cambridge, United Kingdom), 2nd Ed p 194.
4. Lay T, Williams Q, Garnero EJ (1998) The core-mantle boundary layer and deep Earth dynamics. *Nature* 392:461–468.
5. van den Berg AP, Rainey ESG, Yuen DA (2005) The combined influences of variable thermal conductivity, temperature- and pressure-dependent viscosity and core-mantle coupling on thermal evolution. *Phys Earth Planet In* 149:259–278.
6. Lay T, Hernlund J, Buffett BA (2008) Core-mantle boundary heat flow. *Nat Geosci* 1:25–32.
7. Gubbins D, Willis AP, Sreenivasan B (2007) Correlation of Earth's magnetic field with lower mantle thermal and seismic structure. *Phys Earth Planet In* 162:256–260.
8. Dziewonski AM, Anderson DL (1981) Preliminary reference Earth model. *Phys Earth Planet In* 25:297–356.
9. Spiliopoulos S, Stacey FD (1984) The Earth's thermal profile—Is there a mid-mantle thermal-boundary layer?. *J Geodyn* 1:61–77.
10. Shankland TJ, Brown JM (1985) Homogeneity and temperatures in the lower mantle. *Phys Earth Planet In* 38:51–58.
11. Anderson OL (1982) The Earths core and the phase-diagram of iron. *Philos T Roy Soc A* 306:21–35.
12. van der Hilst RD, et al. (2007) Seismostratigraphy and thermal structure of Earth's core-mantle boundary region. *Science* 315:1813–1817.
13. Hofmeister AM (2008) Inference of high thermal transport in the lower mantle from laser-flash experiments and the damped harmonic oscillator model. *Phys Earth Planet In* 170:201–206.
14. Manga M, Jeanloz R (1997) Thermal conductivity of corundum and periclase and implications for the lower mantle. *J Geophys Res-Sol Ea* 102:2999–3008.
15. Lower mantle is composed mainly of silicate perovskite $(Mg, Fe)SiO_3$ (~80% in volume) and magnesiowüstite (Mg,Fe)O (~20% in volume).
16. Charvat FR, Kingery WD (1957) Thermal conductivity: XIII. Effect of microstructure on conductivity of single-phase ceramics. *J Am Ceram Soc* 40:306–315.
17. Slack GA (1962) Thermal conductivity of MgO, Al_2O_3, $MgAl_2O_4$, and Fe_3O_4 crystals from 3 K to 300 K. *Phys Rev* 126:427–441.
18. Touloukian YS, Powell RW, HC Y, KP G (1970) *Thermophysical Properties of Matter—The TPRC Data Series. Thermal Conductivity—Nonmetallic Solids* (IFI/Plenum, New York) p 166.
19. Yukutake H, Shimada M (1978) Thermal-conductivity of NaCl, MgO, Coesite and Stishovite up to 40 Kbar. *Phys Earth Planet In* 17:193–200.
20. Katsura T (1997) Thermal diffusivity of periclase at high temperatures and high pressures. *Phys Earth Planet In* 101:73–77.
21. Andersson S, Backstrom G (1986) Techniques for determining thermal-conductivity and heat-capacity under hydrostatic-pressure. *Rev Sci Instrum* 57:1633–1639.
22. Macpherson WR, Schloessin HH (1982) Lattice and radiative thermal-conductivity variations through high P, T polymorphic structure transitions and melting-points. *Phys Earth Planet In* 29:58–68.
23. Hofmeister AM, Pertermann M, Branlund JM (2007) *Mineral Physicis*, ed Price GD (Elsevier, Netherlands), 543–578.
24. Beck P, et al. (2007) Measurement of thermal diffusivity at high pressure using a transient heating technique. *Appl Phys Lett* 91:181914–181916.
25. In insulating solids, heat conducts mainly via lattice vibrations. Lattice thermal conductivity can well approximate the total thermal conductivity.
26. Cohen RE (1998) Thermal conductivity of MgO at high pressures. *Rev High Pressure Sci Technol* 7:160–162.
27. Tang X, Dong J (2009) Pressure dependence of harmonic and anharmonic lattice dynamics in MgO: A first-principles calculation and implications for lattice thermal conductivity. *Phys Earth Planet In* 174:33–38.
28. Gibert B, Schilling FR, Tommasi A, Mainprice D (2003) Thermal diffusivity of olivine single-crystals and polycrystalline aggregates at ambient conditions—a comparison. *Geophys Res Lett* 30:1046–1051.
29. Callaway J (1959) Model for lattice thermal conductivity at low temperatures. *Phys Rev* 113:1046–1051.
30. Tamura S (1983) Isotope scattering of dispersive phonons in Ge. *Phys Rev B* 27:858–866.
31. Ziman JM (1962) *Eletrons and Phonons: The Theory of Transport Phenomena in Solids* (Oxford Univ Press, Oxford, United Kingdom), pp 287–333.
32. Wu Z, et al. (2008) Pressure-volume-temperature relations in MgO: An ultrahigh pressure-temperature scale for planetary sciences applications. *J Geophys Res-Sol Ea* 113:B06204–B06215.
33. Hofmeister AM (2007) Pressure dependence of thermal transport properties. *Proc Natl Acad Sci USA* 104:9192–9197.
34. Poirier J-P (1991) *Introduction to the physics of the Earth's interior* (Cambridge Univ Press) p 189.
35. Dugdale JS, Macdonald DKC (1955) Lattice thermal conductivity. *Phys Rev* 98:1751–1752.
36. Hofmeister AM (1999) Mantle values of thermal conductivity and the geotherm from phonon lifetimes. *Science* 284:264–264.
37. Jeanloz R, Morris S (1986) Temperature distribution in the crust and mantle. *Annu Rev Earth Pl Sc* 14:377–415.
38. Osako M, Ito E (1991) Thermal-diffusivity of $MgSiO_3$ perovskite. *Geophys Res Lett* 18:239–242.
39. In this composite model of lower mantle, effective thermal conductivity is modeled as $0.2\kappa_{MgO} + 0.8\kappa_{MgSiO_3} = 0.2 \times 43 + 0.8 \times (5.1 \times 43/66) = 11.258$ W/K-m.
40. Clark SP, Jr (1957) Radiative transfer in the Earth's mantle. *Trans Am Geophys Union* 38:931–938.
41. Shankland TJ, Nitsan U, Duba AG (1979) Optical-absorption and radiative heat-transport in olivine at high-temperature. *J Geophys Res* 84:1603–1610.
42. Hofmeister AM (2005) Dependence of diffusive radiative transfer on grain-size, temperature, and Fe-content: Implications for mantle processes. *J Geodyn* 40:51–72.
43. Keppler H, Kantor I, Dubrovinsky LS (2007) Optical absorption spectra of ferropericlase to 84 GPa. *Am Mineral* 92:433–436.
44. Keppler H, Dubrovinsky LS, Narygina O, Kantor I (2008) Optical absorption and radiative thermal conductivity of silicate perovskite to 125 Gigapascals. *Science* 322:1529–1532.
45. Goncharov AF, Struzhkin VV, Jacobsen SD (2006) Reduced radiative conductivity of low-spin (Mg,Fe)O in the lower mantle. *Science* 312:1205–1208.
46. Goncharov AF, Haugen BD, Struzhkin VV, Beck P, Jacobsen SD (2008) Radiative conductivity in the Earth's lower mantle. *Nature* 456:231–234.
47. The single mode excitation approximation simplies the full, self-consistent solution of phonon distribtuion numbers at a non-equilibrium steady state, which is a computationally formidable task for complex mineral sysmtes. It is also known that the single mode excitation approximation does not preserve the property of infinite thermal conductivity in the absence of Umklapp scattering processes (when temperature approaches to zero). However, this difference is expected to be small at high temperatures relevant to the Earth's hot interior.
48. Ziman JM (1962) *Electrons and Phonons: The Theory of Transport Phenomena in Solids* (Oxford Univ Press, Oxford, United Kingdom), pp 285–287.
49. Hofmeister AM (2009) Scale aspects of heat transport in the diamond anvil cell, in spectroscopic modeling, and in Earth's mantle. *Phys Earth Planet In* accepted.